Optics Letters

Passive optical phase noise cancellation

LIANG HU,* XUEYANG TIAN, GUILING WU, AND JIANPING CHEN

State Key Laboratory of Advanced Optical Communication Systems and Networks, Department of Electronic Engineering, Shanghai Jiao Tong University, Shanghai 200240, China
**Corresponding author: liang.hu@sjtu.edu.cn*

Received 18 March 2020; revised 16 June 2020; accepted 25 June 2020; posted 25 June 2020 (Doc. ID 393010); published 29 July 2020

We report on the realization of an optical phase noise cancellation technique by passively embedding the optical phase noise information into a radio frequency signal and creating a copy of the optical frequency signal, which is pre-corrected by the amount of phase noise introduced by optical phase perturbations. Neither phase discrimination nor an active servo controller is required due to the open-loop design, mitigating some technical problems, such as the limited compensation speed and finite phase/timing jitter, in conventional phase noise cancellation. We experimentally demonstrate that this technique maintains the same delay-limited bandwidth and phase noise suppression capability as in conventional techniques, but significantly shortens the response speed and phase recovery time. Passive decoupling optical phase perturbation represents a powerful technique in the domains of optical frequency standard comparisons and tools for future optical atomic clocks, which are now under investigation for a potential redefinition of the International Time Scale.

https://doi.org/10.1364/OL.393010

Clocks ticking at optical frequencies slice time into much finer intervals than do microwave clocks and thus provide unprecedented accuracy, surpassing that of previously available clock systems by more than two orders of magnitude [1–3]. Precise clock networks have the potential to enable dramatic improvements in precision navigation and timing, radio astronomy [4,5], clock-based geodesy [6], testing of fundamental physics [7], geological disaster observation [8], and even future searching for dark matter and gravitational-wave detection [9,10]. At the same time, precision comparisons of different clocks will also be necessary for a future redefinition of the second in the International System of Units (SI) [11,12]. The current well-established, satellite-based techniques for microwave dissemination are not adequate for comparing optical clocks. Taking advantages of the low loss, high stability, large bandwidth, and immunity to electromagnetic interference, the use of optical fiber, today's best optical frequency transfer technique, enables the comparison of state-of-the-art optical atomic clocks and achievement of coherent optical phase transfer over large distances at will, up to thousands of kilometers, preserving their coherence at an extremely high level [13–18].

Optical phase noise in the transmitted frequency introduced by thermal and acoustic fluctuations in the fiber link can be cancelled by either physically modulating the path length or by intentionally shifting the transferred optical frequency. In practical implementations of these methods, the phase variations caused by the changes in the fiber link should be extracted and used to drive tunable devices for phase variation compensation, such as voltage-controlled oscillators (VCOs), as demonstrated by Ma *et al*. in 1994 [13]. The main drawback related to this conventional approach is the need for complex circuits to extract the phase error and drive the devices for phase correction in real time, e.g., frequency dividers with a high ratio needed to extend the phase detection range. Although the method based on VCOs principally has an endless compensation range, achieving short settling time of stabilization locks, namely, a fast compensation speed, is difficult and is a great challenge even for dedicated servo amplifiers. The characteristic of the short settling time is extremely important for the situation, in which signal interruptions frequently occur because of the large signal amplitude fluctuations on long distance fiber links [14–17].

While radio frequency (RF) transfer by multiplexing and dividing the transferred RF signal has been proposed and experimentally demonstrated [19,20], these solutions are not applicable to optical frequency dissemination, in particular, for fiber-based optical frequency dissemination by multiplexing and dividing the transferred optical signal itself. In view of the upcoming redefinition of the second and future applications of optical atomic clocks, technological developments toward more efficient, simple, and robust devices are needed. In this Letter, we propose and demonstrate a novel approach for highly stable dissemination of the phase of an optical frequency reference over an optical-fiber link without any help from the servo electronics. Here neither active phase discrimination nor dynamic phase compensation is required in our open-loop design, enabling the proposed approach to be robust, compact, cost effective, and easy to implement.

Figure 1 depicts a schematic diagram of our optical frequency transfer using a technique with passive phase noise cancellation in an optical fiber. Part of the light with an angular frequency of ν is split off to serve as a local oscillator. The remaining part of this reference light is launched into the link via an acousto-optic modulator 1 (AOM_1) working at an angular frequency of ω_l (downshifted mode, -1 order) and then propagated to the remote end via the optical fiber link, where it encounters AOM_2 (upshifted mode, $+1$ order), which provides a fixed angular

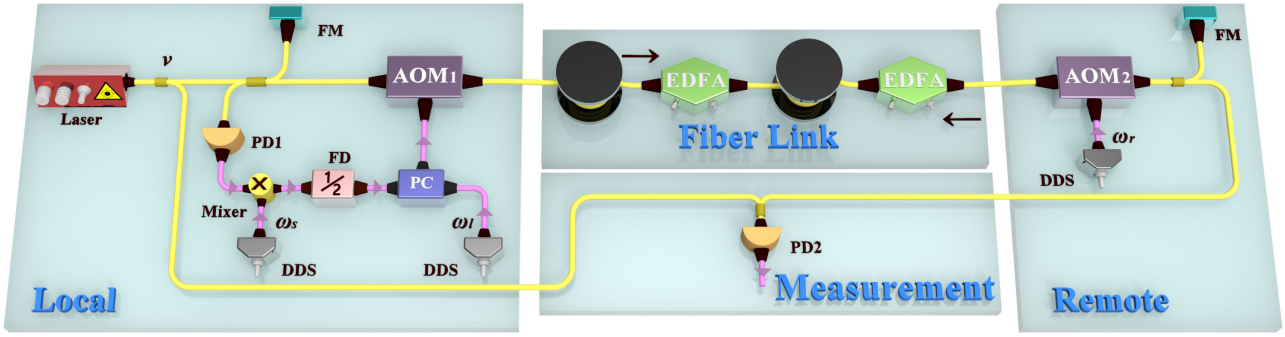

Fig. 1. Schematic diagram of our optical frequency dissemination using a technique with passive phase noise cancellation in an optical fiber. To effectively evaluate the performance of optical frequency dissemination, we measure the beatnote between the phase stabilized optical light at the output of the link with the local reference light obtained by PD2. AOM, acousto-optic modulator; FM, Faraday mirror; DDS, direct-digital synthesizer; EDFA, erbium-doped fiber amplifier; PD, photo-detector; FD, frequency divider; PC, power combiner. Pink and yellow curves represent the electrical and optical signals, respectively.

frequency shift ω_r ($\omega_r > \omega_l$) to distinguish light reflected at the remote end from stray reflections along the link [13]. Most of the light is retroreflected from the remote end via a Faraday mirror, emerges from the start of the fiber, and is heterodyned against the local oscillator light to yield a $2(-\omega_l + \omega_r)$ RF signal with phase noise of $2\phi_p$ at the local photo-detector 1 (PD1). Here, we assume that phase noise ϕ_p in the forward and backward optical paths is equal. Thus, this RF signal includes twice the phase noise of the one-way transmitted optical frequency. To further avoid light reflected at the remote site from stray reflections generated along the fiber link, the detected signal is mixed with an assistant RF signal ω_s ($\omega_s < -\omega_l + \omega_r$), and then the angular frequency of the upper sideband of the mixed signal is used and then divided by a factor of two. Afterwards, its output together with ω_l is fed into the same AOM_1 with the assistance of an RF power combiner, resulting in a desirable optical signal with the angular frequency of $\nu + \omega_l - \omega_r - \frac{1}{2}\omega_s$ and phase $-\phi_p$ at the local site. With this configuration, the first- and third-pass forward optical frequencies differing by $2\omega_l - \frac{1}{2}\omega_s - \omega_r$ follow the same optical path; thus, phase fluctuations caused, for example, by acoustic vibrations or temperature fluctuations are common mode, and do not degrade the optical frequency transfer performance. We carefully engineered the frequency map ($\omega_l, \omega_r, \omega_s$) to ensure that the signals were sufficiently far apart to be easily filtered and separated. Each filtered signal was amplified and tracked using a tracking oscillator with a typical bandwidth of ~100 kHz. In this way, the remote end will automatically receive a stabilized optical frequency signal with an angular frequency of $\nu + \omega_l - \frac{1}{2}\omega_s$.

Note that the above description does not take the propagation delay of the fiber link into account. As noted by Williams *et al.*, the capability of the phase noise rejection will be limited by the fiber propagation delay [18]. The residual phase noise power spectral density (PSD), $S_{\mathrm{remote}}(f)$, at the remote end in terms of the single-pass free-running phase noise PSD, $S_{\mathrm{fiber}}(f)$, and the single-pass fiber propagation delay, τ_0, for our proposed optical frequency transfer can be calculated as

$$S_{\mathrm{remote}}(f) \simeq \frac{1}{3}(2\pi f \tau_0)^2 S_{\mathrm{fiber}}(f). \quad (1)$$

To verify the principle of the proposed scheme, a 145 km optical fiber spool is applied in the laboratory frequency dissemination system. To overcome the one-way attenuation of more than 30 dB, two low-noise erbium-doped fiber amplifier (EDFA) systems are evenly distributed over the entire link length, with the amplifiers located at the middle and end of the fiber link, as depicted in Fig. 1. We built an interferometer by using free-space optics, in which the light can propagate in the optical fiber only when the local oscillator and transferred signal paths are colocated. In comparison with our previous passive temperature stabilized fiber interferometer [21] and active temperature stabilized fiber interferometers in [17,22,23], the out-of-loop phase noise can be easily controlled by using free-space optics [18], which is achieved by simply encapsulating all the components inside an aluminum box filled with foam. Here we set $\omega_l = 45$ MHz, $\omega_r = 75$ MHz, and $\omega_s = 10$ MHz, resulting in out-of-loop beatnotes of 30 MHz and 40 MHz for the free-running link and stabilized link, respectively. All the RF reference signals are provided by a rubidium clock synchronized direct-digital synthesizer (DDS). The frequency selection principle is determined mainly by the bandwidth of AOM_1 and RF bandpass filters. Here, the 3 dB bandwidths of AOM_1 and the RF bandpass filters are ~20 MHz and ~5 MHz, respectively. The beatnotes of the out-of-loop RF signals produced by PD2, as shown in Fig. 1 after electronic amplification and filtering with tracking oscillators, are simultaneously recorded by a dead-time free, high-resolution frequency counter (K + K FXE) operating in Π-type with a gate time of 1 s. The rate of cycle slips is as low as a few per day under typical laboratory conditions, and the signal phase can be continuously tracked for a few days. Routine operation over several days requires regular adjustment of the polarization. As a reference, we measured the residual noise of the interferometer by replacing the fiber spool with a fixed attenuator of equivalent loss and leaving the 1 m patch cord in place, establishing an upper bound of the noise introduced by the interferometer.

Figure 2(a) shows the measured phase noise PSD for the stabilized fiber link (green curve) and the free-running link (black curve), for which no phase noise cancellation was applied. We find that the phase noise PSD of our free-running fiber link approximately follows a power-law dependence, $S_\phi(f) \simeq h_1 f^{-1}\mathrm{rad}^2/\mathrm{Hz}$, for $f < 300$ Hz, indicating that flicker phase noise is dominant in the free-running fiber link, where $h_1 \simeq 65$ in our fiber link. According to the theory of

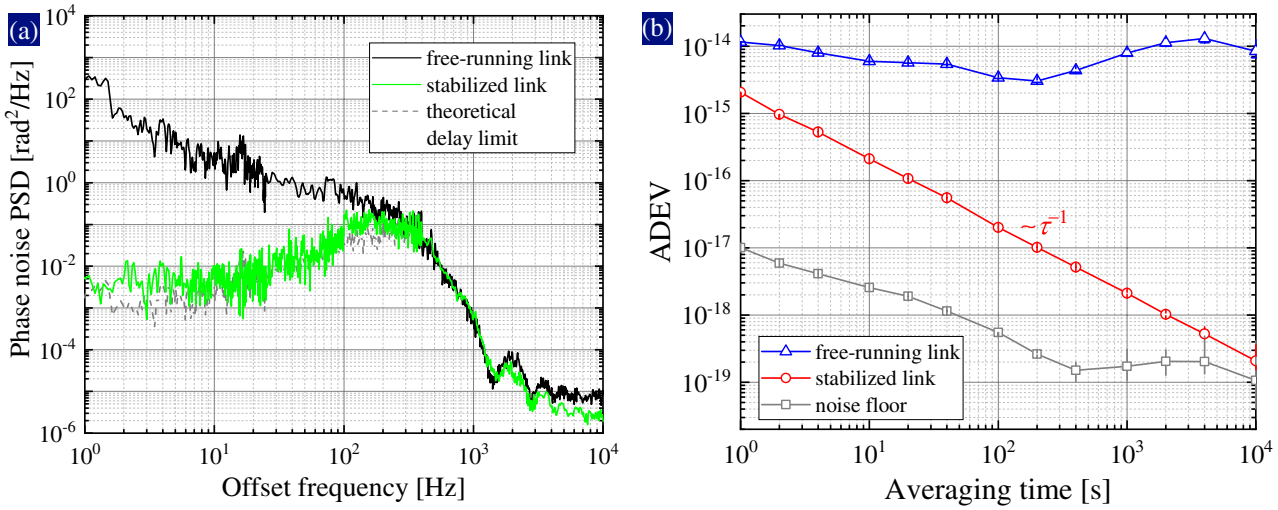

Fig. 2. (a) Measured phase noise PSD of the 145 km free-running fiber link (black curve) and the stabilized link (green curve) with the proposed phase noise cancellation scheme. The gray line is the theoretical prediction based on Eq. (1). (b) Measured fractional frequency instability of the 145 km free-running fiber link (blue triangles) and the stabilized link derived from a nonaveraging (Π-type) frequency counter expressed as the ADEV (red circles). The measured noise floor of the interferometer is also shown (gray squares).

the delay-limited phase noise PSD illustrated in Eq. (1), phase noise cancellation can have the capability to suppress the noise within the delay-limited bandwidth proportional to f^2. Consequently, the residual phase noise of the stabilized link illustrates a $S_\phi(f) = h_3 f^1$ rad^2/Hz dependency with the delay-limited bandwidth of $1/(4\tau_0) \simeq 300$ Hz. In our experiment, $h_3 \simeq 6.3 \times 10^{-4}$. From Fig. 2(a), we also find the measured stabilized phase noise to be in good agreement with the theoretical prediction (gray dashed curve), as indicated in Eq. (1). More importantly, strong servo bumps that appear in the conventional active phase cancellation techniques are eliminated in our phase noise cancellation scheme [15,18]. This is an important characteristic for reducing the integrated phase/timing jitter of the transferred light and preserving the transferred light coherence over a longer fiber link, as discussed in [15,18].

Complementary to the frequency-domain feature, a time-domain characterization of the fractional frequency stability was performed. Figure 2(b) indicates the instability of the free-running link (blue triangles) as well as that of the stabilized link (red circles) expressed as overlapping Allan deviation (ADEV) recorded by a Π-type frequency counter. The data is sampled at a 1 kHz rate and a gate time of 1 s, and therefore, the equivalent measurement bandwidth is 0.5 Hz [24]. The free-running link fluctuates in the 10^{-14} range, with an overall mean of the fractional frequency offset here of $\sim 7.5 \times 10^{-15}$. We obtain a value for the ADEV of 2.1×10^{-15} at 1 s for the stabilized link, which scales down to 2.0×10^{-19} for the integration time of 10,000 s with a slope of τ^{-1}. We note that our results are close to those obtained by field-deployed fiber with a similar fiber length [23,25].

Concerning the frequency accuracy that could not be identified in the instability measurements, we measured the transferred frequency with the Π-type frequency counter with a gate time of 1 s over a period of five days, resulting in a total measurement time of 475,419 s (olive data points, left frequency axis), and calculated the unweighted mean values

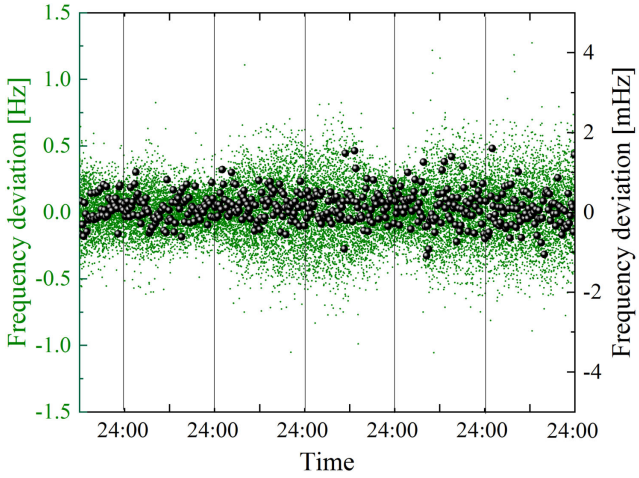

Fig. 3. Five-day frequency comparison between local and remote frequencies after 145 km. Data were taken with dead-time-free Π-type frequency counters with a gate time of 1 s (olive data points, left frequency axis). The arithmetic means of all cycle-slip free 1000 s intervals results in 475 data points (black dots, right frequency axis).

for all cycle-slip free 1000 s long segments, producing 475 data points (black data points, right frequency axis), as shown in Fig. 3. The 475 data points have an arithmetic mean of 12.1 μHz (0.63×10^{-19}) and a standard deviation of 0.46 mHz (2.4×10^{-18}). Considering that the long-term stability is limited mainly by the flicker frequency noise, as shown by the instability expressed by the ADEV shown in Fig. 2(b), we can conservatively constrain the deviations from the expected frequency value to be less than 2.0×10^{-19}, and no frequency bias was observed within the statistical uncertainty of the data set.

Unlike all other optical frequency transfer schemes with conventional phase noise correction, the scheme proposed here can significantly shorten the settling time of stabilization locks. To examine this feature, we implemented two kinds of

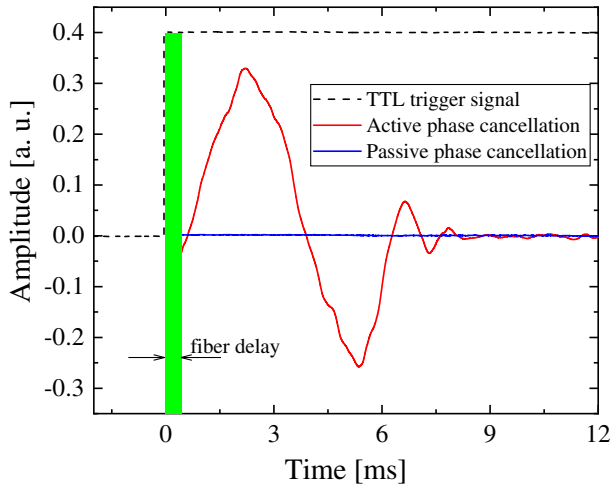

Fig. 4. Phase recovery time of 20 km optical path length stabilization with the proposed and conventional phase noise cancellations, respectively. A delay is introduced between the TTL trigger signal (dashed curve) for switching the light on at 0 ms and the activation of the phase stabilization at $4\tau_0 \simeq 0.4$ ms, as illustrated by the green area. Voltage generated by mixing down the out-of-loop beat to the dc is shown for the switching-on of the active length stabilization for both the conventional (red curve) and proposed (blue curve) phase noise correction techniques.

optical frequency dissemination schemes with the proposed and conventional phase noise cancellations over a 20 km fiber link. The configuration of optical frequency transfer with conventional phase noise correction is similar to that in [14–16], and a high-speed servo controller (Newport, LB1005-S) was used. We observed that the settling time of optical path length stabilization with conventional phase noise cancellation (red curve) is as long as ∼8 ms, whereas the proposed implementation (blue curve) executes much faster settling time limited only by the fiber propagation delay, as depicted in Fig. 4. Consequently, the proposed phase noise cancellation technique has greater capability to recover the stabilized optical signal after the interruptions due to large signal amplitude fluctuations occurring on long distance fiber links than the conventional technique [14–17].

In conclusion, we reported the first noise characterization of optical frequency dissemination over fiber links using passively decoupling optical phase noise introduced by phase perturbations. Only frequency mixing and shifting were used, and no active mechanism was involved, enabling the fiber optical phase transfer system to be compact, cost effective, and easy to implement. As we have shown, this type of optical frequency transfer would allow us to reach the same sensitivity as in the conventional optical frequency transfer techniques but with significantly reduced requirements on electronics. Moreover, we identified the mechanism with fast response speed and phase recovery time behind the proposed phase noise cancellation technique.

Funding. National Natural Science Foundation of China (61905143, 61627817, 61535006); State Grid Corporation of China (SGSHJX00KXJS1901531).

Disclosures. The authors declare no conflicts of interest.

REFERENCES

1. A. D. Ludlow, M. M. Boyd, J. Ye, E. Peik, and P. O. Schmidt, Rev. Mod. Phys. **87**, 637 (2015).
2. W. McGrew, X. Zhang, R. Fasano, S. Schäffer, K. Beloy, D. Nicolodi, R. Brown, N. Hinkley, G. Milani, M. Schioppo, and A. D. Ludlow, Nature **564**, 87 (2018).
3. G. E. Marti, R. B. Hutson, A. Goban, S. L. Campbell, N. Poli, and J. Ye, Phys. Rev. Lett. **120**, 103201 (2018).
4. C. Clivati, R. Ambrosini, T. Artz, A. Bertarini, C. Bortolotti, M. Frittelli, F. Levi, A. Mura, G. Maccaferri, M. Nanni, M. Negusini, F. Perini, M. Roma, M. Stagni, M. Zucco, and D. Calonico, Sci. Rep. **7**, 40992 (2017).
5. B. Wang, X. Zhu, C. Gao, Y. Bai, J. Dong, and L. Wang, Sci. Rep. **5**, 13851 (2015).
6. J. Grotti, S. Koller, S. Vogt, S. Häfner, U. Sterr, C. Lisdat, H. Denker, C. Voigt, L. Timmen, A. Rolland, F. N. Baynes, H. S. Margolis, M. Zampaolo, P. Thoumany, M. Pizzocaro, B. Rauf, F. Bregolin, A. Tampellini, P. Barbieri, M. Zucco, G. A. Costanzo, C. Clivati, F. Levi, and D. Calonico, Nat. Phys. **14**, 437 (2018).
7. C. Lisdat, G. Grosche, N. Quintin, C. Shi, S. Raupach, C. Grebing, D. Nicolodi, F. Stefani, A. Al-Masoudi, S. Dörscher, S. Häfner, J.-L. Robyr, N. Chiodo, S. Bilicki, E. Bookjans, A. Koczwara, S. Koke, A. Kuhl, F. Wiotte, F. Meynadier, E. Camisard, M. Abgrall, M. Lours, T. Legero, H. Schnatz, U. Sterr, H. Denker, C. Chardonnet, Y. L. Coq, G. Santarelli, A. Amy-Klein, R. L. Targat, J. Lodewyck, O. Lopez, and P.-E. Pottie, Nat. Commun. **7**, 12443 (2016).
8. G. Marra, C. Clivati, R. Luckett, A. Tampellini, J. Kronjäger, L. Wright, A. Mura, F. Levi, S. Robinson, A. Xuereb, B. Baptie, and D. Calonico, Science **361**, 486 (2018).
9. S. Kolkowitz, I. Pikovski, N. Langellier, M. D. Lukin, R. L. Walsworth, and J. Ye, Phys. Rev. D **94**, 124043 (2016).
10. L. Hu, N. Poli, L. Salvi, and G. M. Tino, Phys. Rev. Lett. **119**, 263601 (2017).
11. C. Grebing, A. Al-Masoudi, S. Dörscher, S. Häfner, V. Gerginov, S. Weyers, B. Lipphardt, F. Riehle, U. Sterr, and C. Lisdat, Optica **3**, 563 (2016).
12. W. McGrew, X. Zhang, H. Leopardi, R. Fasano, D. Nicolodi, K. Beloy, J. Yao, J. Sherman, S. Schäffer, J. Savory, R. C. Brown, S. Römisch, C. W. Oates, T. E. Parker, T. M. Fortier, and A. D. Ludlow, Optica **6**, 448 (2019).
13. L.-S. Ma, P. Jungner, J. Ye, and J. L. Hall, Opt. Lett. **19**, 1777 (1994).
14. S. Droste, F. Ozimek, T. Udem, K. Predehl, T. W. Hänsch, H. Schnatz, G. Grosche, and R. Holzwarth, Phys. Rev. Lett. **111**, 110801 (2013).
15. D. Calonico, E. K. Bertacco, C. E. Calosso, C. Clivati, G. A. Costanzo, M. Frittelli, A. Godone, A. Mura, N. Poli, D. V. Sutyrin, G. Tino, M. E. Zucco, and F. Levi, Appl. Phys. B **117**, 979 (2014).
16. X. Deng, J. Liu, D.-D. Jiao, J. Gao, Q. Zang, G.-J. Xu, R.-F. Dong, T. Liu, and S.-G. Zhang, Chin. Phys. Lett. **33**, 114202 (2016).
17. S. M. Raupach, A. Koczwara, and G. Grosche, Phys. Rev. A **92**, 021801 (2015).
18. P. A. Williams, W. C. Swann, and N. R. Newbury, J. Opt. Soc. Am. B **25**, 1284 (2008).
19. Y. He, B. J. Orr, K. G. Baldwin, M. J. Wouters, A. N. Luiten, G. Aben, and R. B. Warrington, Opt. Express **21**, 18754 (2013).
20. R. Huang, G. Wu, H. Li, and J. Chen, Opt. Lett. **41**, 626 (2016).
21. L. Hu, X. Tian, G. Wu, M. Kong, J. Shen, and J. Chen, J. Lightwave Technol. **38**, 3644 (2020).
22. F. Stefani, O. Lopez, A. Bercy, W.-K. Lee, C. Chardonnet, G. Santarelli, P.-E. Pottie, and A. Amy-Klein, J. Opt. Soc. Am. B **32**, 787 (2015).
23. G. Grosche, O. Terra, K. Predehl, R. Holzwarth, B. Lipphardt, F. Vogt, U. Sterr, and H. Schnatz, Opt. Lett. **34**, 2270 (2009).
24. S. T. Dawkins, J. J. McFerran, and A. N. Luiten, IEEE Trans. Ultrason. Ferroelectr. Freq. Control **54**, 918 (2007).
25. H. Jiang, F. Kéfélian, S. Crane, O. Lopez, M. Lours, J. Millo, D. Holleville, P. Lemonde, C. Chardonnet, A. Amy-Klein, and G. Santarelli, J. Opt. Soc. Am. B **25**, 2029 (2008).